Single-cell atlas reveals a Wilms' tumor 1-mediated axis driving granulosa cell senescence in human ovarian aging

YANFANG DU[1-3*], CONGYU ZHOU[1-3*], YANPENG TIAN[4], ZHONGKANG LI[1-3] and XIANGHUA HUANG[1-3]

[1]Department of Obstetrics and Gynecology, The Second Hospital of Hebei Medical University, Shijiazhuang, Hebei 050000, P.R. China; [2]Hebei Key Laboratory of Regenerative Medicine of Obstetrics and Gynecology, The Second Hospital of Hebei Medical University, Shijiazhuang, Hebei 050000, P.R. China; [3]National Clinical Key Specialty Construction Project of Gynecology, Shijiazhuang, Hebei 050000, P.R. China; [4]Department of Obstetrics and Gynecology, The First Affiliated Hospital of Zhengzhou University, Zhengzhou, Henan 450052, P.R. China

Received September 16, 2025; Accepted June 9, 2026

DOI: 10.3892/ijmm.2026.5916

Abstract. Ovarian aging is a key cause of reproductive decline in women. Chronic inflammation and granulosa cell (GC) senescence are implicated in this process; however, the underlying cell-type-specific changes and regulatory mechanisms remain incompletely understood. The present study thus aimed to provide insight into these mechanisms. For this purpose, publicly available single-cell transcriptomic data from human ovarian tissues in the Gene Expression Omnibus database (GSE202601) were analyzed, including four young donors (23-29 years of age) and four aged donors (49-54 years of age). Following quality control and integration, clustering, CellChat, pseudotime and SCENIC analyses were performed to define age-related changes in cellular composition, intercellular communication and transcriptional regulation. Key findings were further supported by complementary *in vivo* and *in vitro* experiments in the ovaries of young and aged mice and primary GCs. Integrated analysis revealed marked age-related shifts in ovarian cellular composition, including the enrichment of a pro-inflammatory *NLRP3*$^{+}$ macrophage subpopulation and a senescence-associated GC subtype in aged ovaries. Cell-cell communication analysis suggested enhanced immune-endocrine crosstalk in aged ovaries, with increased IL-1β-IL-1R1 signaling between macrophages and GCs. Pseudotime and transcriptional regulatory network analyses identified Wilms' tumor 1 (*WT1*) as a candidate transcription factor upregulated in aged GCs and positively associated with p21 expression, suggesting a potential role in senescence-associated cell cycle arrest. Experimental validation further supported increased inflammatory signaling, oxidative stress and the activation of the WT1/p21 axis in aged ovaries. On the whole, these findings provide a high-resolution single-cell framework for understanding human ovarian aging and suggest that inflammatory signaling and *WT1*-associated transcriptional reprogramming may contribute to GC senescence and ovarian functional decline.

Introduction

Ovarian aging is a fundamental biological process characterized by a progressive decline in the reproductive capacity of women (1), driven predominantly by the depletion of ovarian follicular reserve, dysregulated steroidogenesis (2) and the progressive remodeling of the stromal microenvironment (3). Clinically, ovarian aging manifests as menstrual irregularity, infertility and, ultimately, menopause. Beyond effects on reproduction, ovarian aging considerably influences systemic health, increasing the risks of developing cardiovascular diseases (4), osteoporosis (5), cognitive decline and overall morbidity in aging women (6). Given its notable role in reproductive and systemic health, a comprehensive understanding of the mechanisms of ovarian senescence is key for developing effective interventions to preserve fertility and enhance the lifelong health of women.

Although inflammation, oxidative stress and apoptosis are established contributors to ovarian aging (7), a considerable number of previous studies have employed bulk tissue analyses, obscuring ovarian cellular heterogeneity and dynamic intercellular interactions (8-11). Consequently, the specific cellular sources and regulatory networks underlying age-related changes, particularly within immune and follicular niches, remain inadequately characterized (12). A cell-type specific understanding is essential to unravel the mechanisms of ovarian senescence. Recent advances in single-cell RNA sequencing (scRNA-seq) permit the high-resolution analysis of complex tissues, revealing cellular diversity, lineage transitions and intercellular communication networks, which were previously

Correspondence to: Professor Xianghua Huang or Dr Zhongkang Li, Department of Obstetrics and Gynecology, The Second Hospital of Hebei Medical University, 215 Heping West Road, Shijiazhuang, Hebei 050000, P.R. China
E-mail: huangxh2022@hebmu.edu.cn
E-mail: zhongkangli@hebmu.edu.cn

*Contributed equally

Key words: ovarian aging, single-cell atlas, WT1, granulosa cells, cellular senescence, inflammatory signaling

undetectable (13). In ovarian aging, scRNA-seq is a powerful tool that can identify cell type-specific alterations, uncover rare senescent subpopulations and define cell-cell interactions involved in functional decline (14). Among ovarian cell types, macrophages have emerged as key immune regulators beyond immune surveillance, influencing tissue remodeling, angiogenesis and follicular development (15). However, their precise phenotypic and functional alterations during ovarian aging, especially interactions with granulosa cells (GCs), remain poorly defined. Clarifying macrophage heterogeneity and signaling roles could illuminate immune-driven inflammatory mechanisms shaping the aging ovarian microenvironment.

Chronic low-grade inflammation is a hallmark of tissue aging and increasingly recognized as a key contributor to ovarian senescence (16). In aged ovaries, macrophages likely serve as both sensors and amplifiers of inflammatory signals, shaping the local microenvironment through cytokine secretion and paracrine interactions (8). GCs, essential for folliculogenesis and steroidogenesis, are particularly sensitive to inflammatory stimuli (17). Emerging evidence suggests that pro-inflammatory macrophage-derived cytokines, such as interleukin (IL)-1β, impair GC function, accelerate follicular atresia and induce premature cellular senescence (18). However, the molecular mechanisms and specific ligand-receptor interactions mediating this macrophage-GC crosstalk remain unclear. Elucidating these interactions is essential for understanding how immune dysregulation impairs GC homeostasis and contributes to the acceleration of ovarian aging.

The progressive decline in GC function during ovarian aging likely results from both extrinsic inflammatory stimuli and intrinsic transcriptional reprogramming (19). Although immune cell-derived paracrine signals may initiate stress responses, sustained GC dysfunction implies deeper transcriptional regulatory changes. However, transcription factors (TFs) orchestrating this senescence-like state remain poorly characterized. Among the TF candidates, Wilms' tumor 1 (*WT1*), a zinc finger TF essential for urogenital development and somatic cell differentiation (20), emerged prominently in the scRNA-seq analyses of ovarian aging which was carried out in the present study. The present study identified *WT1* as the most notably upregulated TF in senescent GCs. Traditionally associated with embryogenesis, recent evidence suggests the reactivation of WT1 in aged tissues and its potential involvement in stress response pathways (21). Its specific role in ovarian aging, particularly in regulating GC fate, remains largely unexplored. Whether WT1 drives GC dysfunction through the activation of downstream targets constitutes a key unresolved question in reproductive aging research.

In the present study, a high-resolution single-cell transcriptomic atlas of human ovaries across reproductive aging was reconstructed. By analyzing publicly available scRNA-seq datasets, age-related cellular composition shifts and intercellular communication dynamics were systemically defined. A pro-inflammatory nucleotide-binding domain, leucine-rich repeat containing family, pyrin domain containing 3 (*NLRP3*)$^{+}$ macrophage subpopulation enriched in aged ovaries and a transcriptionally distinct senescent GC subtype (GC_Aged) were identified. Furthermore, *WT1* emerged as a key transcriptional regulator potentially driving GC senescence via the WT1/p21 axis. Collectively, the findings of the present study elucidate immune-endocrine interplay underlying ovarian aging and establish a detailed cellular and molecular framework for developing novel therapeutic targets to mitigate age-related reproductive decline.

Materials and methods

Animal models and tissue collection. All animal procedures were approved by the Institutional Animal Care and Use Committee of the Second Hospital of Hebei Medical University and performed in compliance with institutional and national guidelines for ethical animal research (approval no. 2021-AE034). Female C57BL/6J mice were purchased from SPAF (Beijing) Biotechnology Co., Ltd., housed under specific pathogen-free conditions with *ad libitum* access to food and water, and maintained on a 12-h light/dark cycle.

A total of 24 mice were used in the present study, including 12 reproductively young mice (3-4 months old) and 12 aged mice (14-18 months old). Following a 7-day acclimatization period, blood and ovarian tissues were collected from young mice at 3-4 months of age and from aged mice at 14-18 months of age. During the study, animal health and behavior were monitored daily, including general appearance, activity, posture, grooming behavior, food and water intake, and signs of pain or distress. Humane endpoints were predefined as severe weight loss, persistent lethargy, inability to access food or water, severe respiratory distress, persistent bleeding, severe infection, or any condition indicating unrelieved pain or suffering. No animals reached the humane endpoints, no animals were found dead prior to the scheduled euthanasia, and all 24 mice were euthanized as planned for tissue collection.

All efforts were made to minimize animal suffering and distress. Mice were maintained under specific pathogen-free housing conditions and handled gently throughout the experiment. For terminal procedures and blood collection, the mice were anesthetized with isoflurane delivered by inhalation at 2% for both induction and maintenance. Blood samples (100-200 μl per mouse) were collected via retro-orbital venous puncture under anesthesia. Ovarian tissues were then collected under aseptic conditions. As these procedures were terminal and performed under anesthesia immediately before euthanasia, post-operative analgesia was not required. Following tissue collection, the mice were euthanized by an overdose of sodium pentobarbital (>150 mg/kg; intraperitoneal), according to AVMA guidelines. Death was verified by confirmation of respiratory arrest, absence of heartbeat, loss of reflexes and the lack of a response to toe pinching prior to disposal.

Harvested ovaries were processed for downstream analyses, including histological staining, western blot analysis, RNA extraction for reverse transcription-quantitative PCR (RT-qPCR) and primary GC isolation for *in vitro* assays, as described below. Collected blood samples were centrifuged at 3,000 x g for 10 min at 4˚C to obtain serum for the measurements of anti-Müllerian hormone (AMH), estradiol (E2) and follicle-stimulating hormone (FSH) levels. As mouse ovarian tissue is limited in size, ovarian samples from the 12 mice in each group were allocated to different downstream assays, including histological staining, immunostaining, RT-qPCR, western blot analysis, hormone assays and primary GC isolation. Western blot analysis was performed using three

independent biological replicates per group with sufficient protein yield, while the remaining samples were used for other experimental validations. These assays are described below.

Primary GC isolation and culture. Primary GC isolation and culture. Primary GCs were isolated from the ovaries of young and aged mice under sterile conditions. Briefly, freshly harvested ovaries were washed with sterile PBS, and the surrounding adipose and connective tissues were carefully removed under a stereomicroscope (Carl Zeiss AG). GCs were mechanically released from visible follicles using a sterile needle and then digested with 0.1% hyaluronidase (Sigma-Aldrich; Merck KGaA) at 37˚C for 5 min. The digestion was terminated by adding complete culture medium. The cell suspension was filtered through a 200-mesh cell strainer, washed twice with PBS, and centrifuged at 300 x g for 5 min at room temperature. The obtained single-cell suspension was cultured in DMEM/F12 medium (1:1; Gibco; Thermo Fisher Scientific, Inc.) supplemented with 10% fetal bovine serum and 1% penicillin-streptomycin at 37˚C in a humidified incubator with 5% CO_2. After 24 h, non-adherent cells and tissue debris were removed by replacing the culture medium. The identity and purity of the isolated GCs were confirmed by follicle-stimulating hormone receptor immunofluorescence staining, and cultures with >95% follicle-stimulating hormone receptor-positive cells were used for subsequent experiments.

Data sources and analytical methods. The scRNA-seq data from human ovarian tissues were obtained from the NCBI Gene Expression Omnibus database under accession number GSE202601 (22). This dataset included samples from 4 reproductively young (23-29 years old) and 4 aged (49-54 years old) women donors with histologically normal ovaries. Raw sequencing data were processed using Seurat (v3.0; Satija Lab, New York Genome Center, New York, NY, USA; https://satijalab.org/seurat/), and low-quality cells were excluded based on gene count thresholds (<200 genes per cell) and mitochondrial RNA content (>10%). Batch effects among samples were corrected using the Harmony algorithm (Broad Institute; https://portals.broadinstitute.org/harmony/). Dimensionality reduction was performed using principal component analysis (PCA), followed by unsupervised clustering using the Louvain method and visualization via UMAP (Uniform Manifold Approximation and Projection; https://umap-learn.readthedocs.io/). Cells were annotated into eight major types based on canonical marker genes and cell-type proportions were compared between age groups.

To explore transcriptional dynamics, pseudotime analysis was conducted using Monocle (v2, Trapnell Lab; https://cole-trapnell-lab.github.io/monocle-release/) to reveal differentiation trajectories and identify genes associated with GC aging. TF activity was inferred using SCENIC (Aerts Lab; https://scenic.aertslab.org/), enabling the reconstruction of regulatory networks and the identification of key regulators. Differential gene expression analysis was performed to compare cellular subpopulations and identify senescence-associated molecular signatures. Functional enrichment analyses of gene sets were assessed using Gene Ontology (GO) and Kyoto Encyclopedia of Genes and Genomes (KEGG) pathways via the clusterProfiler package.

Intercellular communication networks were reconstructed using CellChat (v1.1.3), inferring signaling interactions based on known ligand-receptor pairs. Age-related changes in communication intensity and pathway activation were quantified. Additionally, subclustering analysis was performed to identify key functional cell subsets that were predominantly enriched in aged ovaries.

Clustering and identification of cell types. Single-cell clustering and annotation were performed using Seurat (v3.0). Following data normalization, the top 2,000 highly variable genes were identified using 'FindVariableFeatures' and dimensionality reduction was performed using PCA with the top 20 principal components. Harmony was applied to correct batch effects. Cell clustering was executed using the Louvain algorithm via the 'FindNeighbors' and 'FindClusters' functions (resolution=0.5). Results were visualized using UMAP and t-SNE, implemented in Seurat v3.0.

Differentially expressed genes for each cluster were identified using the Wilcoxon rank-sum test, applying a log fold change cut-off of 0.25 and a minimum expression threshold of 25%. This analysis was used to identify cluster-specific marker genes, which were visualized in the marker gene heatmap shown in the Results below. Cell types were annotated based on cluster-specific markers and established literature. The expression of key genes was visualized using 'FeaturePlot' and 'VlnPlot'. To further dissect functional heterogeneity, key cell types, including GCs and macrophages, underwent subclustering analysis, providing deeper insights into cell-type-specific changes during ovarian aging.

Pseudotime analysis. To explore dynamic transcriptional changes associated with ovarian aging, pseudotime trajectory analysis was performed using Monocle2, focusing on GCs. Highly variable genes were selected to define cell-state transitions and trajectories were constructed using DDRTree for dimensionality reduction. Cells were ordered along pseudotime using the 'orderCells' function and lineage progression was visualized with 'plot_cell_trajectory'. This method enabled identification of differentiation states, key branching points and age-related shifts in gene expression, elucidating the transcriptional progression toward GC senescence.

Transcriptional regulatory network analysis. Transcriptional regulatory networks were reconstructed using the pySCENIC workflow to identify key TFs associated with ovarian aging. The normalized expression matrix obtained from Seurat was utilized as input. Gene regulatory modules were inferred via GRNBoost2, based on TF-target co-expression, followed by *cis*-regulatory motif analysis using RcisTarget with the hg38 motif database. TF-target interactions were filtered to retain only those with enriched binding motifs, forming regulons. Regulon activities across cell types were quantified using regulon specificity scores and network visualization was conducted in Cytoscape. Particular attention was paid to TFs enriched in senescent GCs.

Cell-cell communication analysis. Intercellular communication was assessed using CellChat, which infers signaling interactions based on known ligand-receptor pairs. CellChat

objects were separately created for young and aged samples using normalized expression data. Low-abundance interactions (<10 cells) were filtered out to ensure robustness. Signaling networks were quantified and compared across conditions, focusing on pathway-level differences in frequency and intensity.

EdU assay. To assess cellular proliferation in ovarian tissues, EdU incorporation assays were performed on paraffin-embedded ovarian sections. Female mice were intraperitoneally injected with EdU (50 mg/kg). After 4 h, ovaries were collected, fixed in 4% paraformaldehyde, embedded in paraffin and sectioned at a thickness of 5 μm. The sections were deparaffinized, rehydrated and permeabilized with 0.3% Triton X-100. EdU detection was carried out using the Click-iT™ EdU reaction cocktail containing Azide 555 (Beyotime Biotechnology) according to the manufacturer's instructions. Azide 555 was used as the fluorescent azide reagent to label EdU-positive proliferating cells, which were visualized as red fluorescence. Nuclei were counterstained with Hoechst 33342. Fluorescent signals were visualized under a fluorescence microscope (Carl Zeiss AG) and proliferating cells were quantified based on EdU-positive staining.

TUNEL assay. Apoptotic cells in ovarian sections were detected by TUNEL staining. Samples were fixed in 4% paraformaldehyde, permeabilized with 0.3% Triton X-100 for 25 min at room temperature and incubated with TUNEL reaction mixture (Beyotime Biotechnology) at 37˚C for 2 h in the dark according to the manufacturer's protocol. Nuclei were counterstained with DAPI (SouthernBiotech). Apoptotic cells exhibiting green fluorescence were visualized using a fluorescence microscope (Carl Zeiss AG).

Hematoxylin and eosin (H&E) staining. Histopathological changes were evaluated using H&E staining. Ovarian tissues were fixed in 4% paraformaldehyde, paraffin-embedded and sectioned at a thickness of 5 μm. Sections underwent standard deparaffinization and rehydration, followed by hematoxylin staining for 5 min and eosin staining for 1 min at room temperature using hematoxylin and eosin staining solutions (Wuhan Servicebio Technology Co., Ltd.). Following dehydration and clearing, sections were mounted with neutral balsam. Histological analyses were performed using a light microscope (Carl Zeiss AG) at x200 magnification, focusing on follicular structures and tissue architecture. Images were analyzed with ImageJ software (version 1.53; National Institutes of Health).

Masson's trichrome staining. Masson's trichrome staining was performed to assess collagen deposition and fibrosis in ovarian tissues. Paraffin-embedded sections (5-μm-thick) were deparaffinized, rehydrated and stained using the Masson's Trichrome Staining kit (cat. no. ab150686; Abcam) according to the manufacturer's protocol. Collagen fibers stained blue were visualized under a light microscope (Carl Zeiss AG).

ELISA. Serum levels of anti-Müllerian hormone (AMH), estradiol (E2) and follicle-stimulating hormone (FSH) were measured using commercial ELISA kits (cat. nos. 15775, 1609 and 23789; Meimian Technology Co., Ltd.) following the manufacturer's instructions. Briefly, 50 μl serum samples were added per well, incubated with HRP-conjugated antibodies provided in the ELISA kits (cat. nos. 15775, 1609 and 23789; Meimian Technology Co., Ltd.) at 37˚C for 30 min, and subsequently reacted with substrate solution. Following reaction termination, absorbance at 450 nm was measured using a microplate reader (BioTek Epoch). Hormone concentrations were calculated based on standard curves.

Immunohistochemistry staining. Immunohistochemistry was performed on paraffin-embedded mouse ovarian tissue sections to detect NLRP3 and p21 expression. Briefly, ovarian tissues were fixed in 4% paraformaldehyde at room temperature for 48 h, embedded in paraffin and cut into 5-μm-thick sections. The sections were deparaffinized, rehydrated and subjected to antigen retrieval using sodium citrate buffer (Wuhan Servicebio Technology Co., Ltd.). Endogenous peroxidase activity was blocked with 3% hydrogen peroxide, and the sections were blocked with 5% goat serum for 30 min at room temperature. The sections were then incubated overnight at 4˚C with primary antibodies against NLRP3 (1:200; cat. no. AG-20B-0014; AdipoGen Life Sciences) or p21 (1:200; cat. no. ab109520; Abcam). After washing with PBS, the sections were incubated with the corresponding HRP-conjugated secondary antibody for 30 min at 37˚C. Immunoreactivity was visualized using diaminobenzidine (DAB; ZSGB-BIO), and nuclei were counterstained with hematoxylin staining solution (Wuhan Servicebio Technology Co., Ltd.) for 1 min at room temperature. Images were captured using a light microscope (Carl Zeiss AG), and the scale bars are indicated in the corresponding figure legends.

RT-qPCR. Total RNA was extracted from ovarian tissues and GCs using TRIzol® reagent (Invitrogen; Thermo Fisher Scientific, Inc.). RNA concentration and purity were evaluated using a NanoDrop spectrophotometer. cDNA synthesis was performed using MonScript™ RTIII All-in-One Mix with dsDNase (Monad Biotech Co., Ltd.). qPCR was conducted using GoTaq® qPCR Master Mix (Promega Corporation) on a Bio-Rad CFX96 system under the following cycling conditions: 95˚C for 10 min, followed by 40 cycles at 95˚C for 15 sec and 60˚C for 60 sec. Gene expression was normalized to *GAPDH* and analyzed using the $2^{-\Delta\Delta Cq}$ method (23). The primer sequences used for RT-qPCR are listed in Table SI.

Western blot analysis. Protein expression was determined using western blot analysis. Ovarian tissues and GCs were lysed in RIPA buffer (Beyotime Biotechnology) supplemented with protease and phosphatase inhibitors. Protein concentrations were quantified using a BCA assay (Beyotime Biotechnology). Equal amounts of protein (30 μg) were separated by 10% SDS-PAGE and transferred onto PVDF membranes. Membranes were blocked in 5% non-fat milk diluted in TBS-Tween at room temperature for 1 h and incubated overnight at 4˚C with primary antibodies against superoxide dismutase 1 (SOD1; 0.2 μg/ml; cat. no. ab13498; Abcam), isocitrate dehydrogenase 1 (IDH1; 1:1,000; ab230949; Abcam), glutathione S-transferase P 1 (GSTP1; 1:1,000; ab153949; Abcam), NLRP3 (1:1,000; cat.

no. ab270449; Abcam), IL-1β (1:1,000; cat. no. ab254360; Abcam), pro-IL-1β (1:1,000; cat. no. ab254360; Abcam), apoptosis-associated speck-like protein containing a CARD (ASC; formerly known as PYCARD; 1:1,000; cat. no. ab151700; Abcam), WT1 (1:100; cat. no. ab224806; Abcam), p21 (1:1,000; cat. no. ab109199; Abcam), p16 (1:2,000; cat. no. ab211542; Abcam) and GAPDH (1:200,000; cat. no. ab181602; Abcam). Following three washes with TBS-Tween (TBS-T) for 10 min each, the membranes were incubated with HRP-conjugated secondary antibodies, including goat anti-rabbit IgG H&L (HRP; 1:5,000; cat. no. ab97051; Abcam), for 1 h at room temperature. Bands were visualized using enhanced chemiluminescence (Thermo Fisher Scientific, Inc.) and densitometric analysis was performed using ImageJ software (version 1.53; National Institutes of Health).

As mouse ovarian tissue is limited in size, tissues from the 12 mice in each group were allocated to different downstream assays, including histological staining, immunostaining, RT-qPCR, western blot analysis, hormone assays, and primary GC isolation. Western blot analysis was performed using three independent biological replicates per group with sufficient protein yield.

Immunofluorescence staining. To identify primary GCs, follicle-stimulating hormone receptor (FSHR) immunofluorescence staining was performed. Briefly, cultured GCs were fixed with 4% paraformaldehyde, permeabilized with 0.3% Triton X-100 (Beijing Solarbio Science & Technology Co., Ltd.) and blocked with 5% goat serum (Wuhan Servicebio Technology Co., Ltd.) for 1 h at room temperature. The cells were then incubated overnight at 4˚C with rabbit anti-mouse FSHR antibody (1:200; cat. no. GB11275-1; Wuhan Servicebio Technology Co., Ltd.). After washing with PBS, the cells were incubated with Alexa Fluor 488-conjugated goat anti-rabbit IgG secondary antibody (1:200; cat. no. GB25303; Wuhan Servicebio Technology Co., Ltd.) for 1 h at room temperature in the dark. Nuclei were counterstained with DAPI (SouthernBiotech) for 10 min at room temperature. The staining was observed using a fluorescence microscope (Carl Zeiss AG).

For ovarian tissue immunofluorescence staining, paraffin-embedded mouse ovarian sections (5-μm-thick) were deparaffinized, rehydrated and subjected to antigen retrieval using sodium citrate buffer (pH 6.0). The sections were permeabilized with 0.3% Triton X-100 (Beijing Solarbio Science & Technology Co., Ltd.) for 25 min at room temperature and blocked with 5% goat serum (Wuhan Servicebio Technology Co., Ltd.) for 30 min at room temperature. The sections were then incubated overnight at 4˚C with anti-WT1 antibody (1:100; cat. no. ab224806; Abcam). After washing with PBS, the sections were incubated with Alexa Fluor 488-conjugated goat anti-rabbit IgG secondary antibody (1:200; cat. no. GB25303; Wuhan Servicebio Technology Co., Ltd.) for 1 h at room temperature in the dark. Nuclei were counterstained with DAPI (SouthernBiotech) for 10 min at room temperature. The sections were mounted with antifade mounting medium and images were captured using a fluorescence microscope (Carl Zeiss AG). The scale bars are indicated in the corresponding figure legends.

Senescence-associated β-galactosidase staining. Senescence-associated β-galactosidase staining was performed to evaluate cellular senescence in primary GCs using a Senescence β-Galactosidase Staining kit (Beyotime Biotechnology) according to the manufacturer's instructions. Briefly, primary GCs isolated from young and aged mouse ovaries were seeded into six-well plates. After washing with PBS, the cells were fixed with β-galactosidase staining fixative for 15 min at room temperature. The cells were then washed with PBS and incubated with freshly prepared β-galactosidase staining solution at 37˚C overnight in a dry incubator without CO_2. Positive cells exhibiting blue staining were observed using a light microscope (Carl Zeiss AG). The proportion of senescence-associated β-galactosidase-positive cells was calculated from randomly selected fields.

Statistical analysis. Statistical analyses were conducted using GraphPad Prism (version 9.0; GraphPad Software; Dotmatics). Data are expressed as the mean ± SD. For comparisons between two groups, two-tailed unpaired Student's t-tests were used. For comparisons among three or more groups, ANOVA followed by Tukey's post hoc test was performed. A value of $P<0.05$ was considered to indicate a statistically significant difference. Each experiment was independently repeated at least three times, and the number of biological replicates used for each assay is indicated in the corresponding Methods section or figure legends. Data visualization was conducted using bar charts, violin plots and box-and-whisker plots as appropriate, ensuring reproducibility and reliability of quantitative findings.

Results

Construction of a single-cell atlas of human ovarian aging. To characterize the cellular landscape of human ovarian aging, publicly available single-nucleus RNA sequencing data (GSE202601) derived from ovarian tissues of 4 aged donors (49-54 years of age) and 4 young donors (23-29 years of age) without known reproductive disorders were analyzed. Rigorous quality control procedures were applied to ensure analytical robustness and biological relevance (Fig. S1). Cells with <200 detected genes or with mitochondrial RNA content >10% were excluded (Fig. S1A). The Seurat and Harmony pipelines were used for data normalization, batch correction and integration (Fig. S1B), followed by dimensionality reduction and clustering. Highly variable genes were identified and visualized to support downstream analyses, confirming substantial transcriptomic variability across the dataset (Fig. S1C). Cell-cycle analysis indicated no systematic bias across samples (Fig. S1D). UMAP projections revealed consistent cellular identities between the young and aged groups and across all eight samples (Fig. S1E and F). In addition, a heatmap of gene expression patterns further supported the reproducibility and integrity of the dataset (Fig. S1G). In total, 42,261 high-quality cells were retained and classified into eight major cell types, including smooth muscle cells, theca cells, macrophages, fibroblasts, stromal cells, endothelial cells, GCs and epithelial cells, with cell-type proportions summarized in Fig. S1H.

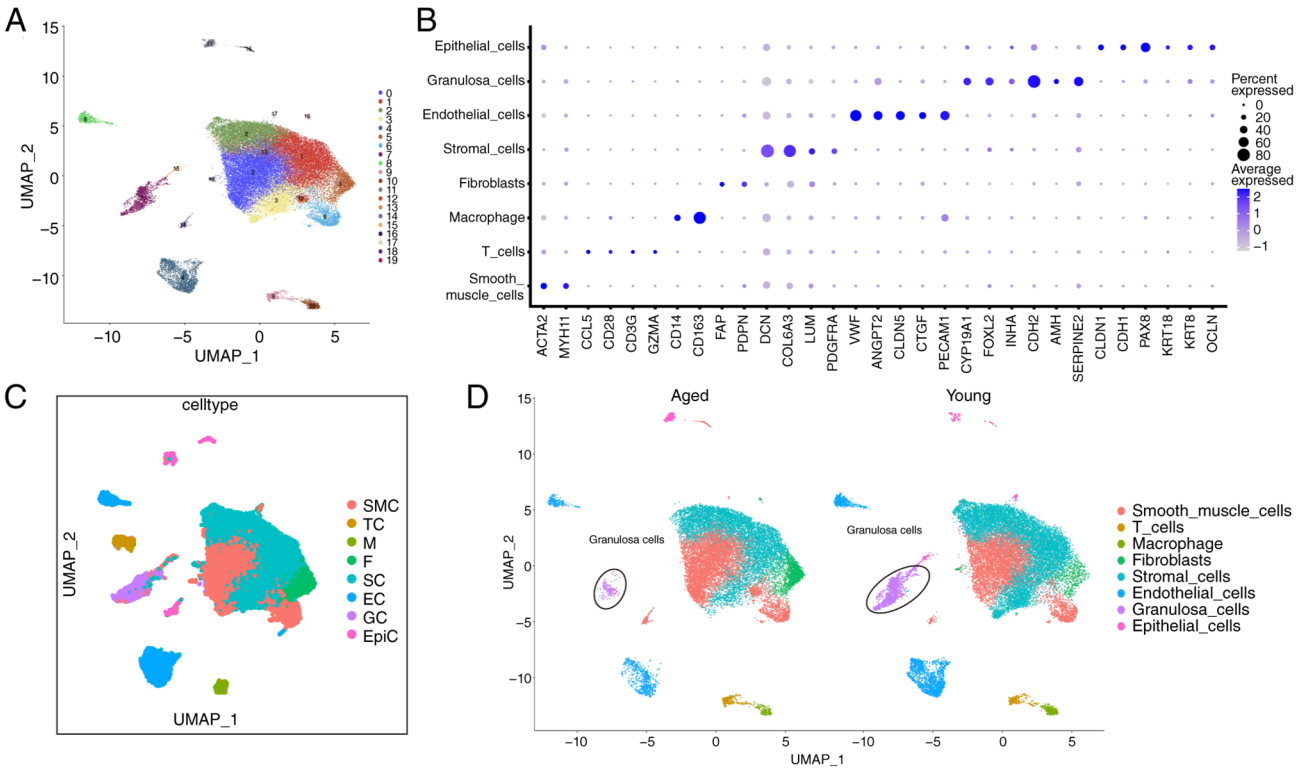

Figure 1. Construction of a single-cell atlas of human ovarian aging. (A) UMAP plot of 42,261 single-nucleus transcriptomes from young and aged human ovarian tissues, revealing 20 transcriptionally distinct clusters. (B) Dot plot illustrating the expression of canonical marker genes across eight annotated ovarian cell types, including GCs, theca cells, macrophages, epithelial cells, fibroblasts, smooth muscle cells, stromal cells and T-cells. Dot size indicates the proportion of expressing cells, and color intensity indicates average expression. (C) UMAP plot colored by annotated cell type identity. (D) UMAP projections of young and aged ovarian samples shown separately, highlighting age-associated shifts in cellular composition, including reduced GC abundance in aged ovaries. GCs, granulosa cells; TC, theca cells; M, macrophages; EpiC, epithelial cells; F, fibroblasts; SMC, smooth muscle cells; SC, stromal cells.

Unsupervised clustering identified 20 transcriptionally distinct clusters across all samples (Figs. 1A and S2A). Based on canonical marker gene expression, these clusters were annotated as GCs, theca cells, macrophages (M), epithelial cells, fibroblasts (F), smooth muscle cells, stromal cells and T-cells (Figs. 1B and C, and S1H). Marker-based classification was supported by the lineage-specific expression of genes, such as *CYP19A1* and *CDH2* in GCs, *CLDN1* and *PKP3* in epithelial cells, *VWF* and PECAM1 in endothelial cells, and *PDPN* and *FAP* in fibroblasts, as visualized using the FeaturePlot function in Seurat based on normalized single-cell expression data (Fig. 2A). Violin plots demonstrated lineage-specific marker expression (Fig. 2B) and heatmap analysis of differentially expressed genes further supported robust cluster identity assignment (Fig. 2C). Comparative UMAP projections and compositional analysis revealed a clear reduction in GCs and a relative increase in fibroblasts and epithelial cells in aged ovaries (Figs. 1D and 2D). These changes were consistently observed across individual donor samples (Fig. S2A and B), confirming the reproducibility of age-associated cellular remodeling. Collectively, these analyses establish a high-resolution single-cell atlas of the human ovary and provide a foundation for subsequent identification of aging-associated cellular and molecular alterations.

Age-associated cellular remodeling and inflammatory/oxidative stress signatures. To further assess inflammation and oxidative stress-related changes associated with ovarian aging, the expression levels of key inflammatory and antioxidant regulators were analyzed. The inflammasome component, *NLRP3*, a hallmark of chronic inflammation, together with antioxidant-related genes including *SOD1, PRDX1, GSTP1* and *SOD3,* were specifically examined based on normalized single-cell transcriptomic data (Fig. S3). UMAP projections, dot plots violin plots based on normalized single-cell transcriptomic data revealed a significantly increased expression of *NLRP3* in aged ovaries, particularly within macrophages (Fig. S3A-C). By contrast, multiple antioxidant genes, most notably *SOD1,* exhibited a significantly reduced expression in aged ovaries, particularly within endothelial and GC populations (Fig. S3D-F). These observations suggest that ovarian aging is accompanied by inflammatory activation and impaired antioxidant defense, which may together contribute to functional decline within the aged ovarian microenvironment.

Enhanced macrophage-granulosa cell communication and increased IL-1β signaling in aged ovaries. Earlier histological analyses indicated a prominent expression of NLRP3 surrounding follicles in aged ovaries, suggesting that macrophages may influence GC function through inflammasome activation. To test this hypothesis, a comprehensive intercellular communication analysis was performed using CellChat on integrated single-cell transcriptomic data. Overall, aged ovarian tissues exhibited notably increased intercellular communication, reflected by the enhanced number and strength of interactions (Fig. 3A). Comparative

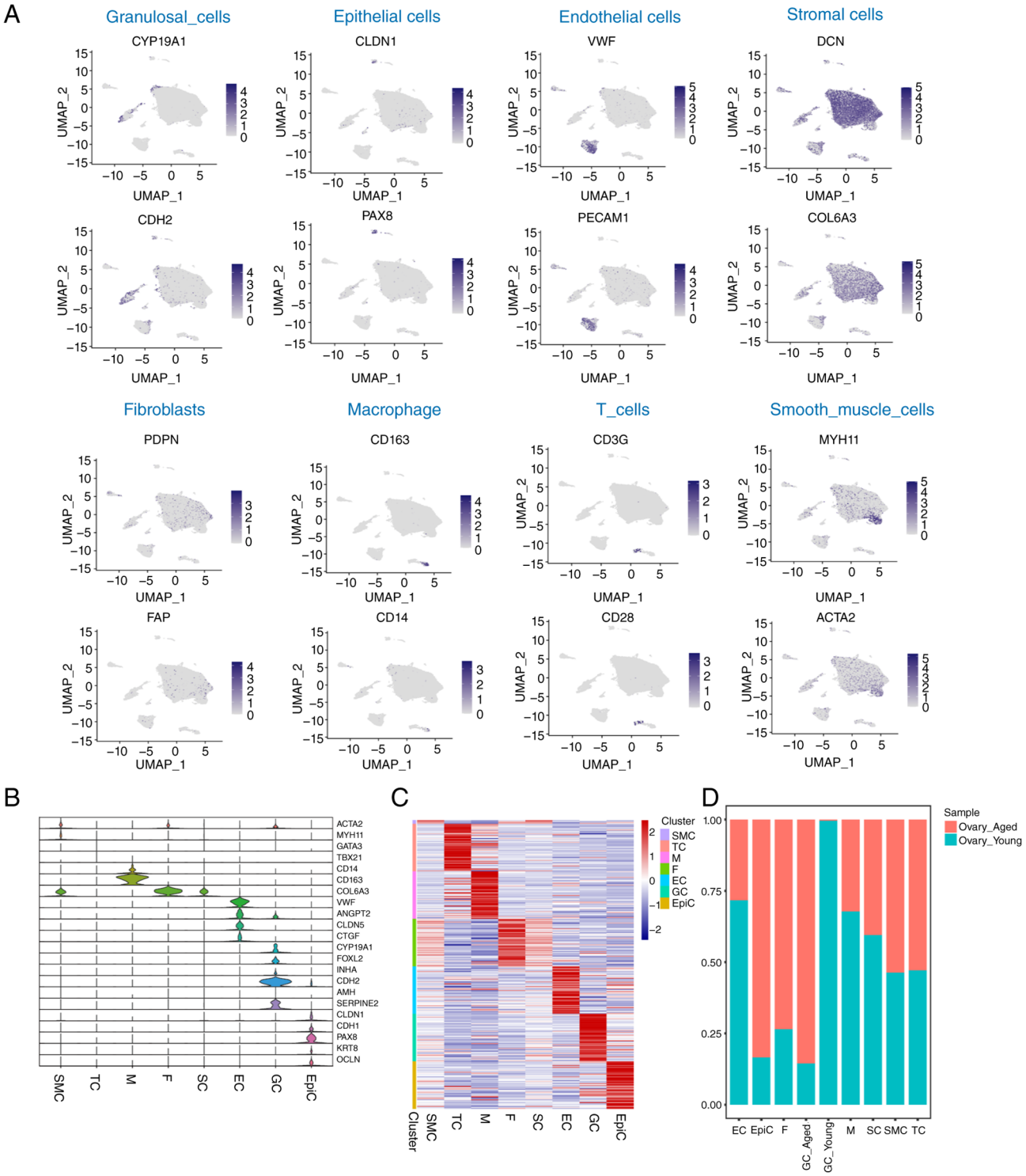

Figure 2. Marker-based annotation and cell-type composition of human ovarian aging. (A) Feature plots demonstrating representative marker gene expression used to define major ovarian cell types. (B) Violin plots displaying expression levels of selected marker genes across cell types. (C) Heatmap of differentially expressed genes across cell types, validating transcriptional identities. (D) Bar plot illustrating the relative proportions of each cell type in young vs. aged ovaries. GC, granulosa cell; TC, theca cell; M, macrophage; EpiC, epithelial cell; F, fibroblast; SMC, smooth muscle cell; SC, stromal cell; EC, endothelial cell.

analyses revealed that aged ovaries possessed 196 unique interaction events compared with 130 in young ovaries, with total interaction strength more than doubling (4.673 vs. 2.275). Macrophage interactions were substantially amplified across multiple cell types in aged ovaries, particularly with GCs (Fig. 3B). These increased interactions were both more frequent and stronger, indicative of active signaling exchange. Chord diagrams further emphasized intensified macrophage-granulosa-stromal cell interactions in aged ovaries (Fig. 3C). Pathway-level analyses revealed significant age-related changes in signaling activity, notably pronounced IL-1β signaling. CellChat analysis predicted that macrophages were the predominant source of IL-1β signaling, with GCs representing a notable target population in aged ovaries

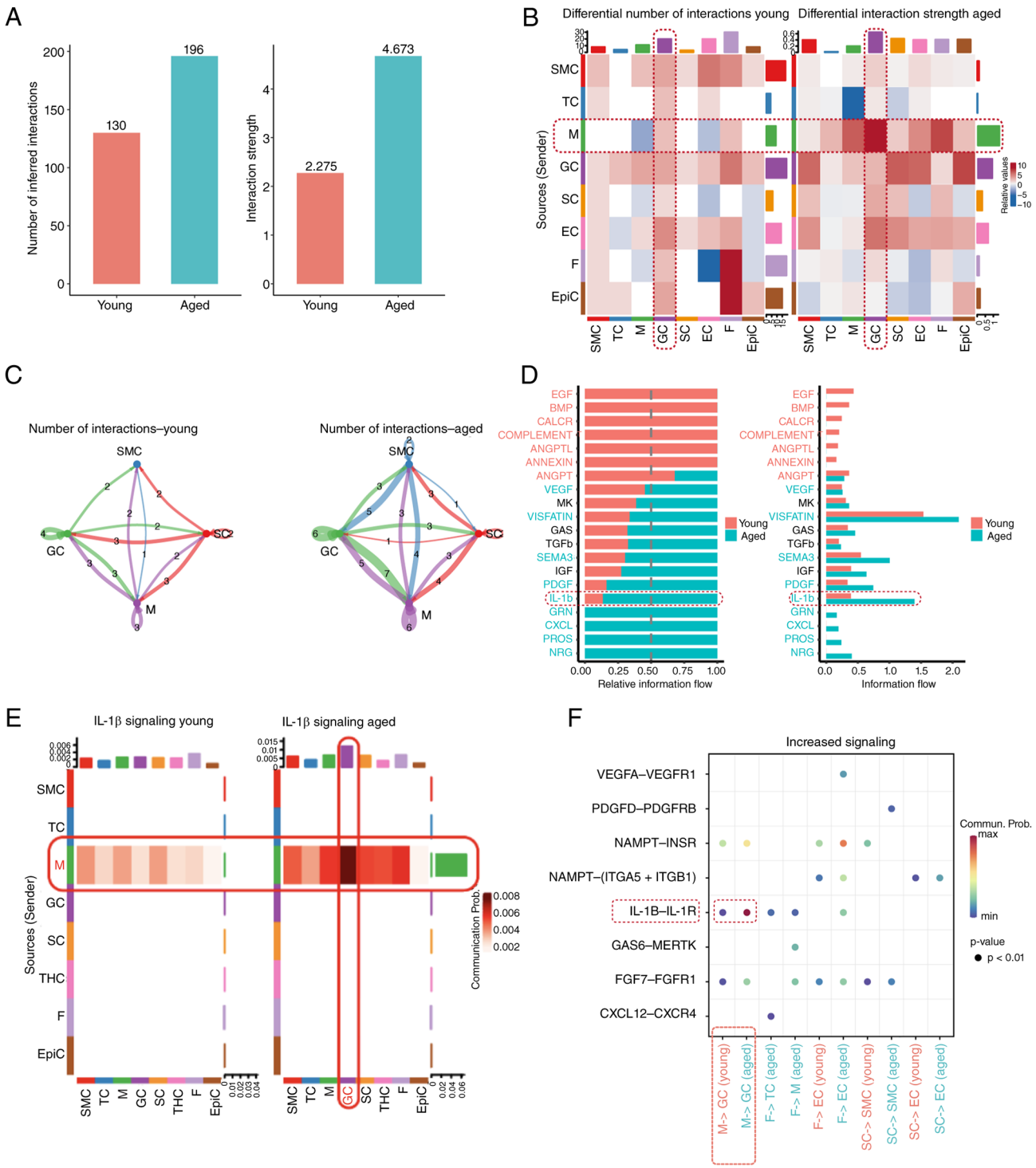

Figure 3. Enhanced macrophage-granulosa cell communications and increased IL-1β signaling in aged ovaries. (A) Bar plots illustrating the number and total strength of intercellular interactions in young and aged ovaries. (B) Heatmaps displaying differential interaction number (left panel) and interaction strength (right panel) between cell types. (C) Chord diagrams illustrating the number of interactions among major cell types in young (left panel) and aged (right panel) ovaries. (D) Bar plots illustrating age-dependent changes in pathway-level signaling, including relative and absolute information flow. (E) Heatmaps of IL-1β signaling interactions across cell types in young (left panel) and aged (right panel) ovaries. (F) Dot plot illustrating increased IL-1β-IL-1R1 ligand-receptor signaling between macrophages and granulosa cells in aged ovaries. Circle size and color intensity reflect communication probability.

(Fig. 3D and E). Communication heatmaps indicated that IL-1β signaling was negligible in young ovaries but highly active in aged samples, specifically from macrophages to GCs (Fig. 3E). Ligand-receptor pair analysis further suggested enhanced IL-1β-IL-1R1 signaling between macrophages and GCs in aged ovaries (Fig. 3F).

To further characterize the global intercellular signaling landscape, cell-cell communication was categorized and analyzed for age-related alterations. Among pathways upregulated with aging, fibroblast growth factor (FGF), platelet-derived growth factor (PDGF), and insulin-like growth factor (IGF) signaling exhibited pronounced

activation, particularly signals originating from stromal, endothelial and fibroblast populations targeting granulosa and epithelial cells (Fig. S4A). Detailed FGF pathway analysis demonstrated enhanced signaling intensity and expanded sender-receiver relationships in aged ovaries, notably from fibroblast and stromal cells to granulosa and epithelial cells (Fig. S4B). These changes reflect augmented tissue remodeling and potentially disrupted follicular support. Receptor ligand analyses further highlighted elevated signaling interactions, specifically involving FGF7-FGFR1, CXCL12-CXCR4, GAS6-MERTK and NAMPT-INSR pairs in aged ovaries, indicative of a pro-inflammatory and pro-fibrotic microenvironment (Fig. S4C). Collectively, these findings suggest that macrophage-associated inflammatory signaling, together with broader remodeling of intercellular communication networks, may contribute to fibrosis, altered angiogenesis and disrupted follicular function during ovarian aging.

Identification and characterization of a pro-inflammatory NLRP3$^+$macrophage subpopulation in aged ovaries. Macrophages represent the predominant immune cell population within the ovarian microenvironment and exhibit significant heterogeneity. To investigate age-associated shifts in macrophage identity, ovarian macrophages were re-clustered based on single-cell transcriptomic profiles. This analysis revealed three distinct macrophage subclusters, with cluster 0 predominantly derived from aged ovaries (Fig. 4A). This cluster exhibited an elevated expression of *NLRP3*, indicative of inflammasome activation and was thus designated as a pro-inflammatory *NLRP3*$^+$ macrophage subpopulation (Fig. 4B and C). The GO and KEGG enrichment analyses of differentially expressed genes within this subpopulation highlighted enrichment in IL signaling and monocyte differentiation pathways, indicating a pro-inflammatory immune phenotype during aging (Fig. 4D). Pseudotime trajectory analysis demonstrated that aged macrophages represent terminally differentiated cells derived from younger counterparts, with progressively increased *NLRP3* expression along pseudotime (Fig. 4E and F). These findings suggest that *NLRP3*$^+$ macrophages emerge with aging and may represent an important inflammatory macrophage subpopulation in the aged ovary.

To further support these observations, mouse ovarian tissues enriched for macrophages were examined. Aged ovarian tissues exhibited a significantly increased expression of NLRP3, ASC and pro-IL-1β, indicating elevated inflammasome activity and pro-inflammatory cytokine production (Fig. 4G and H). Taken together, these results support the distinct molecular identity of the *NLRP3*$^+$ macrophage subset and suggest its potential involvement in age-associated ovarian inflammation.

Identification and functional characterization of a senescent GC subpopulation in aged ovaries. To clarify age-related transcriptional heterogeneity within GCs, subclustering analysis was performed using single-cell transcriptomic data. This analysis delineated GCs into eight distinct clusters (Fig. 5A). Cluster 4 predominantly originated from aged ovaries and displayed substantial transcriptional divergence (Fig. 5A and B). Based on functional and senescence-associated gene expression, GCs were categorized into GC_Young (functional GCs) and GC_Aged (senescence-like GCs) subtypes (Fig. 5C).

The GC_Aged subtype was enriched in aged ovaries and exhibited a reduced expression of key functional markers, such as *NR5A2, LINGO2* and *RIMS2*, along with an increased expression of aging-related genes, including *LAMA2* and *ADAMTS9-AS2*. By contrast, the proportion of GC_Young cells declined markedly in aged ovaries, whereas GC_Aged became the predominant subtype (Fig. 5D). UMAP visualizations further confirmed a reduced expression of *NR5A2*; this is critical for steroidogenesis and an increased expression of *LAMA2*, which is associated with extracellular matrix remodeling and senescence, in GCs from aged ovaries (Fig. 5E).

To validate these observations experimentally, primary GCs were isolated from young and aged mouse ovaries. Immunofluorescence staining confirmed >95% FSHR positivity, indicating high purity of the cultured GCs (Fig. 5F). Senescence-associated β-galactosidase staining exhibited a significantly higher proportion of senescent cells in GCs from aged ovaries (Fig. 5G). Collectively, these results identify and characterize a previously unrecognized GC_Aged subpopulation with senescence-associated features, suggesting that GC aging may be a key contributor to ovarian functional decline.

Pseudotime and transcription factor analysis identifies WT1 as a candidate regulator of granulosa cell senescence. To further elucidate the molecular mechanisms underlying GC aging, pseudotime trajectory and SCENIC transcription factor analysis was performed. Pseudotime mapping revealed clear temporal differences between young and aged GCs, with aged cells primarily located at the terminal differentiation state (Fig. 6A and B). SCENIC analysis identified age-specific transcriptional regulators. In aged GCs, transcription factor activity scores for WT1, NRF2 and KLF2 were significantly increased compared with young cells, with WT1 ranking among the top age-associated regulators (Fig. 6C). Gene activity heatmaps confirmed the upregulation of *WT1* regulons in aged samples.

Spatial and quantitative analysis further demonstrated the specificity of *WT1* expression in aged GCs. t-SNE and violin plots demonstrated that *WT1* was predominantly expressed in granulosa and fibroblast populations of aged ovaries, whereas it was almost absent in young ovries (Fig. 6D and E). Notably, *WT1* expression was positively associated with p21, a key cell cycle inhibitor associated with cellular senescence (Fig. 6F). These findings suggest that *WT1* may be associated with GC aging and may contribute to the upregulation of p21 in aged GCs.

Experimental validation of aging-associated ovarian changes and WT1/p21 activation. To elucidate the histological and molecular hallmarks of ovarian aging, ovaries from reproductively young (3-4 months old) and aged (14-18 months old) C57BL/6J mice were compared. Aged ovaries displayed prominent degenerative features, including reduced cell proliferation, increased apoptosis and fibrosis, disrupted endocrine function, elevated oxidative stress and heightened inflammatory signaling. Specifically, proliferative capacity was assessed by EdU incorporation assays, which revealed a significant decline in GC proliferation in aged ovaries

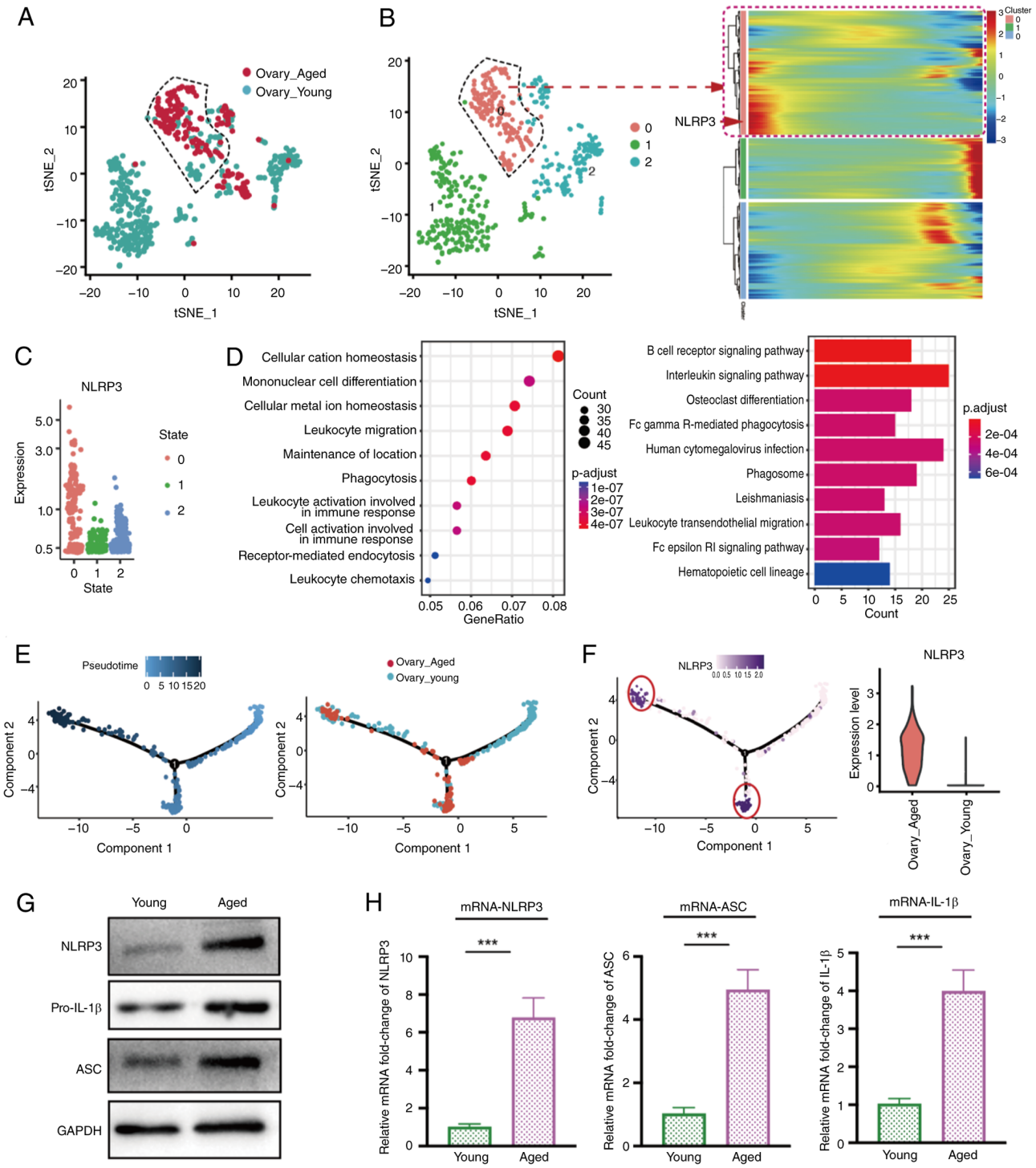

Figure 4. Identification and characterization of a pro-inflammatory *NLRP3*$^{+}$ macrophage subpopulation in aged ovaries. (A) t-SNE plot demonstrating three transcriptionally distinct macrophage subclusters, with cluster 0 predominantly enriched in aged ovaries. (B) t-SNE and heatmap analyses illustrating an elevated expression of *NLRP3* in cluster 0. (C) Scatter plot showing the distribution of NLRP3 expression across macrophage subclusters, with higher NLRP3 expression observed in cluster 0. (D) Gene Ontology and Kyoto Encyclopedia of Genes and Genomes enrichment analyses of cluster 0-specific genes, highlighting pathways related to interleukin signaling and monocyte differentiation. (E) Pseudotime trajectory illustrating the developmental progression of macrophages, with aged macrophages occupying a terminal state. (F) Pseudotime expression dynamics illustrating the progressive upregulation of *NLRP3*, together with a violin plot demonstrating the increased expression of *NLRP3* in aged samples. (G) Western blot analysis of NLRP3, pro-IL-1β and ASC in young and aged mouse ovarian tissues. (H) Reverse transcription-quantitative PCR analysis demonstrating increased mRNA levels of *NLRP3*, *ASC* and *IL-1β* in aged samples. Data are presented as the mean ± SEM. ***P<0.001. Western blot images shown are representative of three independent biological replicates per group. NLRP3, nucleotide-binding domain, leucine-rich repeat containing family, pyrin domain containing 3; ASC, apoptosis-associated speck-like protein containing a CARD (ASC; formerly known as PYCARD.

(Fig. 7A). TUNEL staining further indicated increased apoptosis in aged follicles, confirming enhanced cellular attrition (Fig. 7B). Histological examination by H&E staining demonstrated a marked decrease in the number of follicles at all developmental stages in aged ovaries (Fig. 7C; lower panel). Quantitative hormone analysis revealed significantly

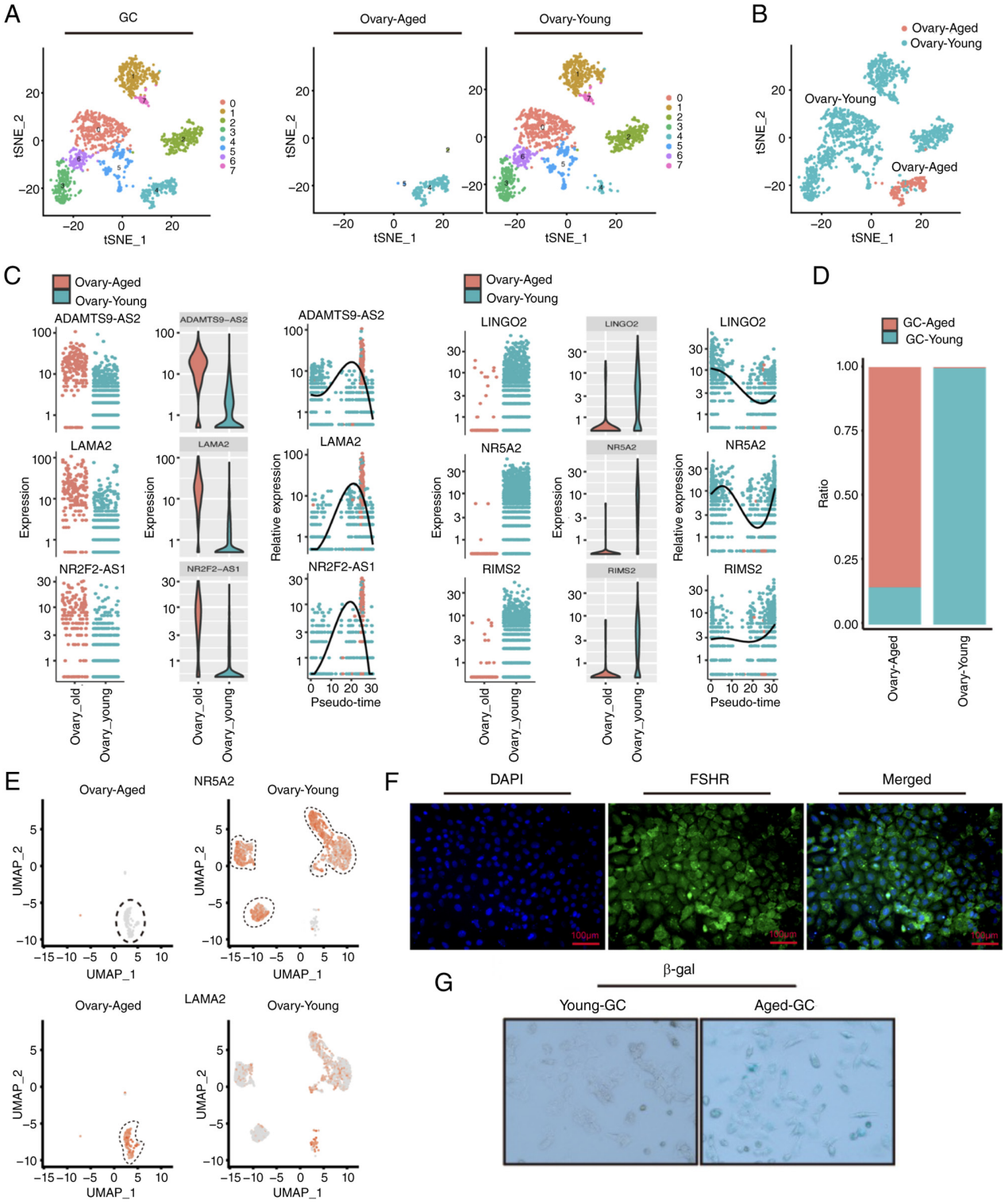

Figure 5. Identification and functional characterization of a senescent GC subpopulation in aged ovaries. (A) t-SNE plots demonstrating granulosa cell clustering into eight transcriptionally distinct subclusters, with cluster 4 enriched in aged ovaries. (B) t-SNE plots highlighting the distribution of granulosa cells from young and aged ovaries. (C) Expression profiles of functional genes (*NR5A2*, *LINGO2*, and *RIMS2*) and senescence-associated genes (*LAMA2* and *ADAMTS9-AS2*) in GC_Young and GC_Aged subtypes. (D) Bar plot demonstrating subtype composition in young and aged ovaries, indicating predominance of GC_Aged in aged samples. (E) UMAP plots illustrating increased *LAMA2* expression and reduced *NR5A2* expression in aged granulosa cells. (F) Immunofluorescence staining for FSHR confirming granulosa cell identity in primary cultures; nuclei were counterstained with DAPI. Scale bar, 100 μm. (G) Senescence-associated β-galactosidase staining demonstrating increased cellular senescence in granulosa cells isolated from aged ovaries. GC, granulosa cell; FSHR, follicle-stimulating hormone receptor.

reduced serum levels of AMH and E2, along with elevated FSH levels in aged mice, reflecting diminished ovarian reserve and endocrine function (Fig. 7D).

Masson's trichrome staining revealed increased collagen deposition in aged ovaries, consistent with fibrotic remodeling of the ovarian stroma (Fig. 7E). Immunohistochemistry

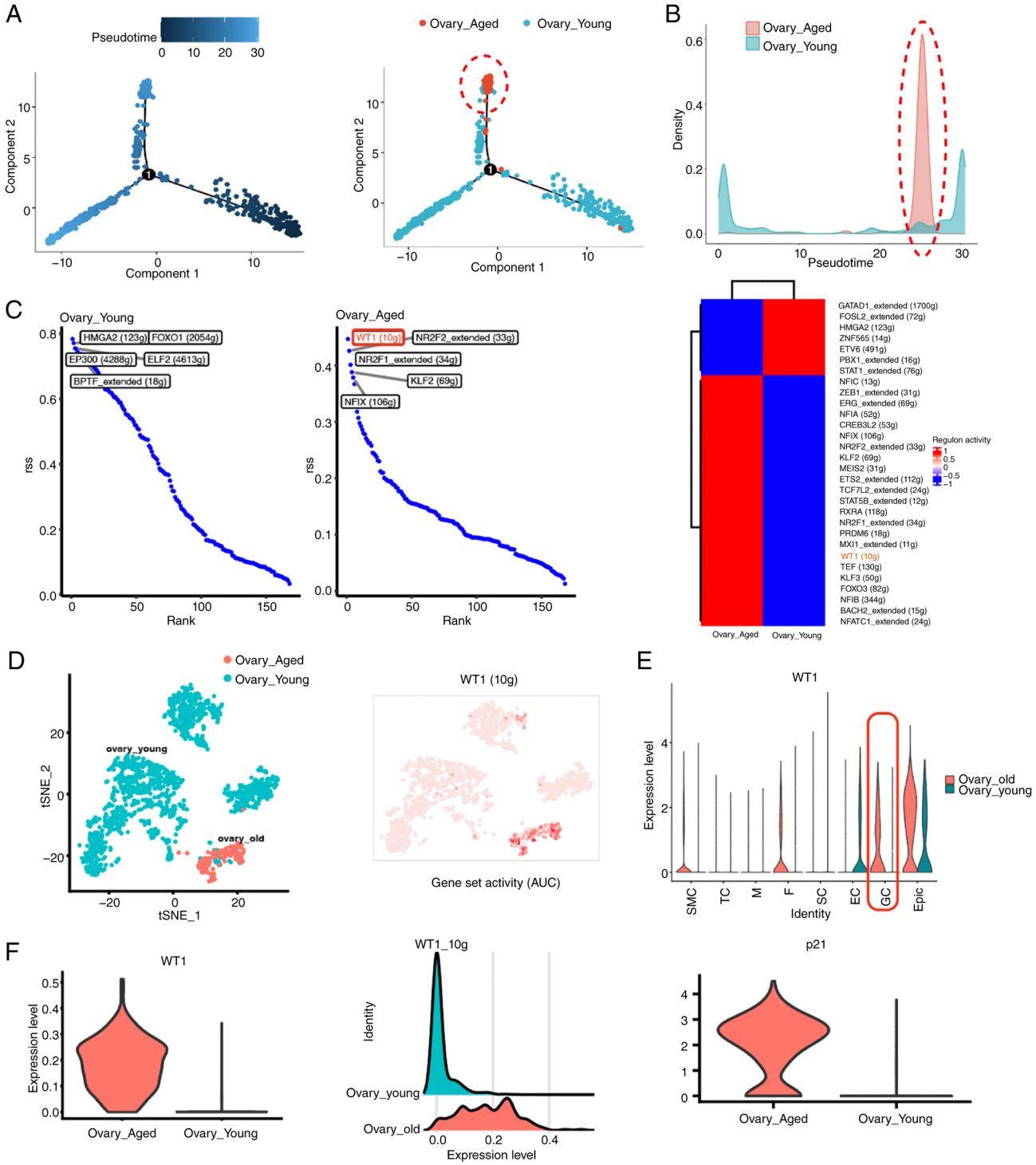

Figure 6. Pseudotime and SCENIC analyses identify WT1 as a candidate regulator of granulosa cell senescence. (A) Pseudotime trajectory analysis of granulosa cells showing aged cells concentrated at terminal differentiation states. (B) Density distribution of young and aged granulosa cells along pseudotime. (C) SCENIC analysis identifying transcription factors with increased activity in aged granulosa cells, with WT1 among the top age-associated regulators. (D) t-SNE plots illustrating the increased expression of *WT1* in aged granulosa cells. (E) Violin plots illustrating elevated *WT1* expression in granulosa and fibroblast populations of aged ovaries. (F) Co-expression analysis illustrating a positive association between *WT1* and p21 in aged granulosa cells.

demonstrated enhanced expression of the inflammasome component NLRP3, particularly localized around aging follicles (Fig. 7F). Western blot analysis confirmed the down-regulation of key antioxidant enzymes (SOD1, IDH1 and GSTP1) in aged ovaries (Fig. 7G), alongside the upregulation of the inflammatory mediators NLRP3 and IL-1β (Fig. 7H). These changes were further corroborated at the transcriptional level, as RT-qPCR analysis revealed the significantly decreased mRNA expression of *SOD1* and *GSTP1*, and the increased expression of *NLRP3* and *Il1β* in aged ovarian tissues (Fig. 7I). Collectively, these findings delineate the core characteristics of ovarian aging, including reduced cell proliferation, follicular depletion, fibrotic tissue remodeling, oxidative stress and chronic inflammation.

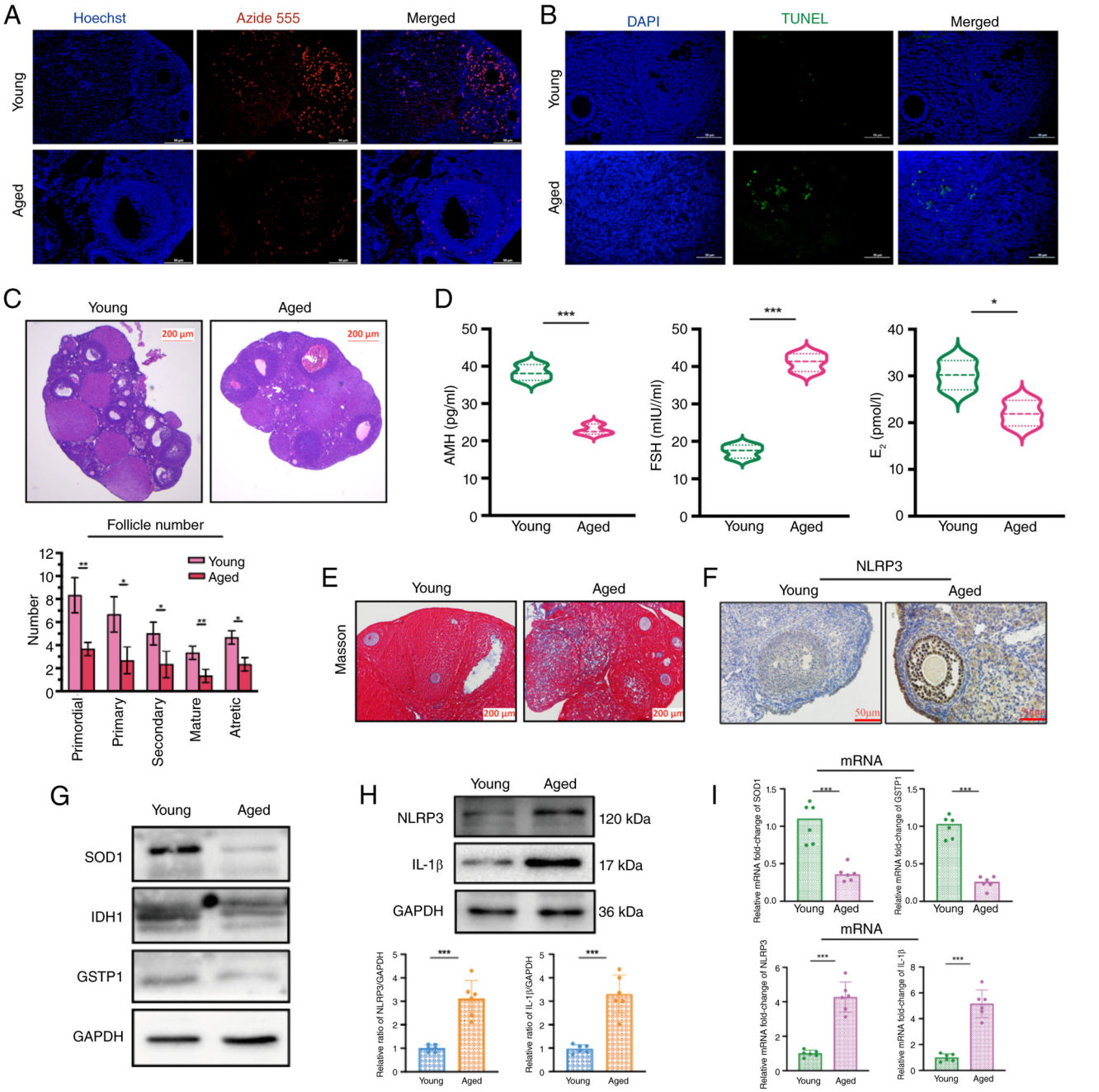

Figure 7. Experimental validation of aging-associated ovarian changes in mice. (A) EdU immunofluorescence staining (Azide 555, red) and Hoechst nuclear staining (blue) showing reduced granulosa cell proliferation in aged ovaries. Scale bar, 50 μm. (B) TUNEL staining showing increased apoptotic cell death in aged ovarian tissues; nuclei were counterstained with DAPI (blue). Scale bar, 50 μm. (C) Representative hematoxylin and eosin-stained ovarian sections and quantitative analysis of follicle counts at different developmental stages (primordial to atretic). Scale bar, 200 μm. (D) Serum AMH, FSH and E2 levels measured using ELISA in young and aged mice. (E) Masson's trichrome staining showing enhanced fibrosis in aged ovaries. Scale bar, 200 μm. (F) Immunohistochemical staining showing increased NLRP3 expression in follicles of aged ovaries. Scale bar, 50 μm. (G) Western blot analysis demonstrating the decreased expression of antioxidant enzymes SOD1, IDH1 and GSTP1 in aged ovaries. (H) Western blot analysis demonstrating the increased expression of NLRP3 and IL-1β in aged ovaries, with densitometric quantification normalized to GAPDH. (I) Reverse transcription-quantitative PCR analysis demonstrating the decreased mRNA expression of *SOD1* and *GSTP1*, and the increased expression of *NLRP3* and *IL-1β* in aged ovarian tissues. Data are presented as the mean ± SEM. *P<0.05, **P<0.01 and ***P<0.001. Experiments shown in were independently repeated at least three times. Western blot analyses (G and H) were performed using at least three independent biological replicates per group. Western blot images shown are representative of three independent biological replicates per group. NLRP3, nucleotide-binding domain, leucine-rich repeat containing family, pyrin domain containing 3; IDH1, isocitrate dehydrogenase 1; GSTP1, glutathione S-transferase P 1.

To further validate the WT1-p21 regulatory axis *in vivo*, protein and mRNA levels of WT1 and p21 in GCs isolated from aged and young mouse ovaries were examined. Western blot analysis confirmed a marked increase in WT1 and p21 protein levels in aged GCs (Fig. 8A). Immunohistochemistry further revealed the elevated expression of p21, specifically within the GC layer of aged ovarian follicles (Fig. 8B). Immunofluorescence analysis revealed the widespread upregulation of WT1 in aged ovarian tissues (Fig. 8C). Additionally, RT-qPCR results demonstrated significantly higher *WT1* and

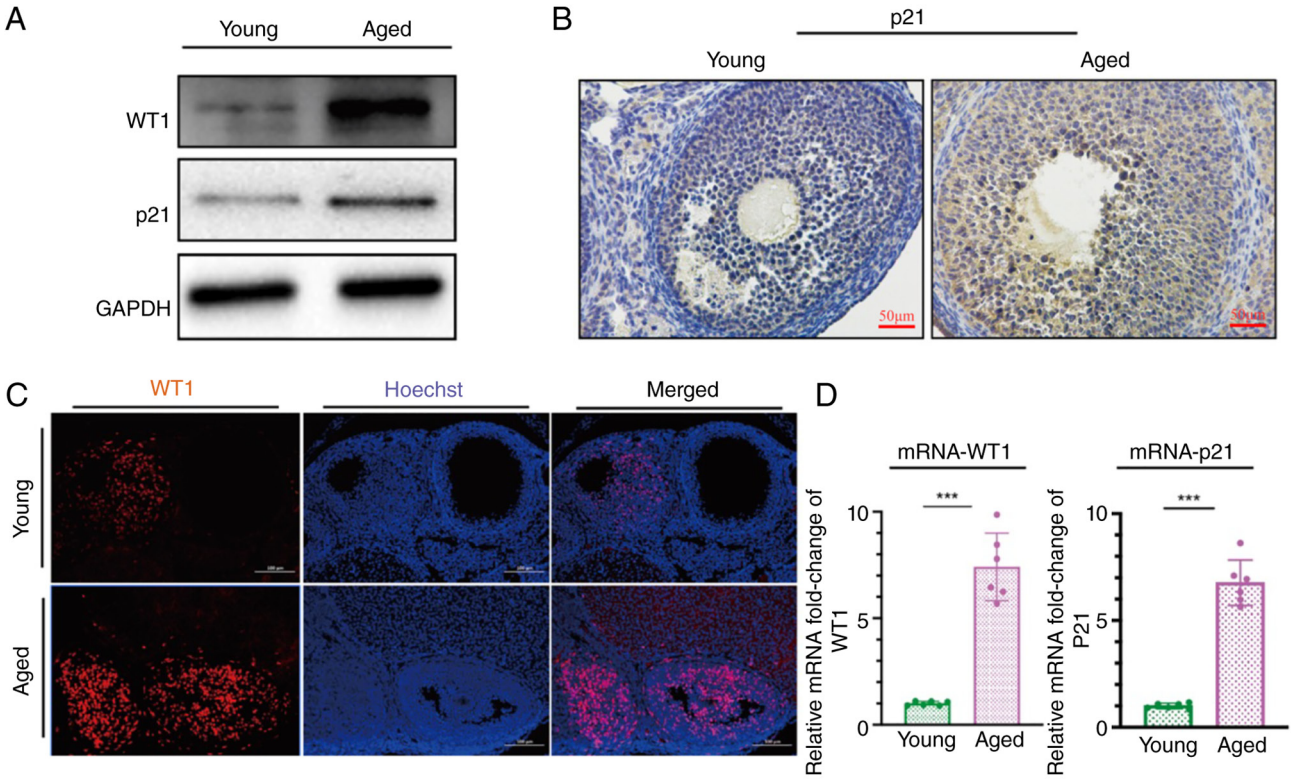

Figure 8. *In vivo* validation of WT1/p21 activation in aged ovarian granulosa cells. (A) Western blot analysis showing increased WT1 and p21 protein levels in aged granulosa cells. (B) Immunohistochemistry illustrating the elevated expression of p21 in the granulosa cell layer of aged ovarian follicles. Scale bar, 50 μm. (C) Immunofluorescence staining illustrating increased WT1 expression in aged ovarian tissues; nuclei were counterstained with Hoechst. Scale bar, 100 μm. (D) Reverse transcription-quantitative PCR analysis demonstrating the increased mRNA levels of *WT1* and *CDKN1A* (p21) in aged ovaries. Data are presented as mean ± SEM. ***P<0.001. Experiments shown were independently repeated at least three times. Western blot analysis (A) was performed using three independent biological replicates per group. Western blot images shown are representative of three independent biological replicates per group.

CDKN1A (p21) mRNA expression in aged ovaries compared with young controls (Fig. 8D). Taken together, these results support the presence of a WT1/p21-associated expression pattern that may be involved in GC senescence and age-related ovarian decline.

Discussion

The present study presents a comprehensive single-cell transcriptomic atlas of human ovarian aging, elucidating key cellular and molecular alterations associated with reproductive senescence. Notably, two aging-associated subpopulations were identified: Pro-inflammatory 'NLRP3^{+}' macrophages and senescent 'GC_Aged' GCs. Enhanced IL-1β/IL-1R1 signaling between these cell types, together with the upregulation of WT1 in aged GCs, supports a potential association between chronic inflammation and transcriptional reprogramming during ovarian functional decline.

The identification of a distinct NLRP3+ macrophage subpopulation enriched in aged ovaries, characterized by the increased expression of pro-inflammatory genes and increased IL-1β/IL-1R1-related signaling with GCs, aligns with previous research demonstrating the age-associated upregulation of NLRP3 inflammasome components and IL-1β in ovarian tissues, contributing to diminished fertility (24). The enhanced macrophage-GC communication observed suggests that NLRP3-associated inflammatory signaling may contribute importantly to ovarian aging. This finding highlights the potential of targeting the NLRP3 inflammasome pathway as a therapeutic strategy to mitigate age-related ovarian decline.

A transcriptionally distinct GC_Aged subpopulation was predominant in aged ovaries, exhibiting the downregulation of functional markers, such as NR5A2 and the upregulation of senescence-associated genes, including LAMA2 and p21. These findings corroborate those of previous studies indicating that GC senescence markedly contributes to ovarian aging and dysfunction (25,26). Herein, *in vitro* assays confirmed the senescent phenotype of GC_Aged cells through β-galactosidase staining and the elevated protein expression of p21, reinforcing that intrinsic GC aging is key in ovarian functional decline. The accumulation of senescent GCs has also been implicated in conditions, such as polycystic ovary syndrome, where the increased expression of p16 and p21 disrupts folliculogenesis (27). In the present study, WT1 emerged as a pivotal transcription factor upregulated in aged GCs, with SCENIC and pseudotime analyses confirming its significant activation. The positive association between WT1 and p21 expression suggests that WT1 may be associated with GC senescence and may participate in the regulation of cell-cycle arrest-related pathways. These results were further corroborated by western blot analysis, immunofluorescence and RT-qPCR analyses, confirming the upregulation of WT1 and p21 at the transcript and protein levels in aged ovaries. Traditionally recognized for its role in urogenital development (28), the reactivation of WT1 in aged tissues and its involvement in cellular stress responses suggest a broader role

in cellular aging processes. The observed upregulation of WT1 in aged GCs, together with the increased expression of p21, suggests that WT1 may be involved in GC senescence, thereby extending the understanding of transcriptional reprogramming in ovarian aging.

The present study highlights the potential importance of immune-endocrine crosstalk in ovarian aging, particularly the increased IL-1β/IL-1R1 signaling observed between macrophages and GCs. This interaction suggests chronic inflammation mediated by immune cells markedly contributes to ovarian functional decline. Recent studies have shown that aging ovaries exhibit an increased infiltration of immune cells, including macrophages, secreting pro-inflammatory cytokines, such as IL-1β and TNF-α, impairing GC function and disrupting folliculogenesis and steroidogenesis (7,29). The identification of the NLRP3^{+} macrophage subpopulation enriched in aged ovaries further supports the involvement of inflammatory mechanisms in ovarian aging and raises the possibility of an inflammatory feedback process contributing to GC dysfunction. This finding aligns with the findings of previous research demonstrating the role of the NLRP3 inflammasome in age-related inflammation and tissue degeneration (30).

Recent single-cell studies of ovarian aging provide a key framework for interpreting the findings of the present study across species and experimental contexts. Isola *et al* (31) constructed a single-cell atlas of the aging mouse ovary and reported age-associated shifts in granulosa and stromal cell populations, accompanied by the activation of senescence-related transcriptional programs. These observations are consistent with the identification, in the present study, of a senescent GC subpopulation in aged human ovaries, suggesting that GC aging represents a conserved feature across species. In addition, Zhou *et al* (32) recently described a pro-inflammatory macrophage subset undergoing pyroptosis in aged human ovaries, which promotes follicular dysfunction through IL-1β signaling. The results of the present study similarly highlight enhanced immune GC communication and inflammatory signaling during ovarian aging. However, rather than focusing on macrophage pyroptosis, the present study further identified WT1-mediated transcriptional reprogramming within GCs, suggesting an additional downstream mechanism associating inflammation with cellular senescence. Furthermore, a single-cell atlas of primate ovarian aging reported conserved aging-related features, including oxidative stress, mitochondrial dysfunction and immune infiltration (33). These cross-species findings support the present study observation of increased inflammatory signaling and immune endocrine crosstalk in aged human ovaries. Taken together, these comparisons indicate that immune activation and GC dysfunction are conserved features of ovarian aging across species, while the present study extends current knowledge by identifying a WT1-mediated transcriptional regulatory axis that may contribute to GC senescence in human ovarian aging.

The integration of high-quality scRNA-seq data from human ovaries provides a robust perspective on ovarian aging, enabling the identification of conserved cellular and molecular changes associated with aging and thereby enhancing the translational relevance of the present study findings. Multi-modal validation through western blotting, RT-qPCR and histological staining further supports the reliability of the present study. However, several limitations should be acknowledged. Although the analyses in the present study suggested that enhanced IL-1β/IL-1R1 signaling in aged ovaries may be associated with NLRP3+ macrophages and GC_Aged GCs, subgroup-specific cell-cell communication analysis and direct *in vitro* co-culture validation were not performed in the present study. Therefore, this proposed inflammatory crosstalk should be considered a preliminary, data-driven inference that requires further validation. This was mainly as NLRP3^{+} macrophages and GC_Aged cells were identified by secondary subclustering, and further stratification by age group and subcluster identity resulted in relatively limited cell numbers and sparse ligand-receptor expression in some subgroup combinations. Under these conditions, subgroup-specific CellChat inference may be unstable and potentially misleading.

A further limitation of the present study is the absence of direct functional perturbation experiments, such as WT1 knockdown or the inhibition of IL-1β/NLRP3 signaling. Therefore, although the data of the present study support the involvement of inflammatory signaling and the WT1/p21-associated axis in ovarian aging, the causal roles of these pathways in granulosa cell senescence and ovarian aging remain to be established. While p21 was examined as a key mediator of cell cycle arrest and senescence, other cell cycle-related proteins were not evaluated in the present study. Future studies incorporating a broader panel of cell cycle regulators will be necessary to further clarify the role of the WT1/p21-associated axis in granulosa cell senescence during ovarian aging. Moreover, although WT1 expression was positively associated with CDKN1A (p21) and both were upregulated in aged GCs, a direct transcriptional regulatory relationship was not demonstrated. Due to these limitations, the causal roles of these pathways in GCs senescence and ovarian aging remain to be established. Additionally, the limited human sample size may affect the generalizability of these findings and warrants validation in larger cohorts. Although the findings were supported by multiple *in vivo* and *in vitro* experiments, validation using human ovarian tissues remains necessary to further confirm the translational relevance of these results. Future studies incorporating human ovarian samples will help strengthen the clinical applicability of the identified WT1-mediated regulatory axis.

Future research is required to focus on functional studies targeting the key regulators identified in the present study. Future studies incorporating subgroup-resolved communication analysis and macrophage-GC co-culture systems are warranted to validate the proposed inflammatory crosstalk more directly. In addition, targeted perturbation approaches, including WT1 knockdown and the blockade of IL-1β/NLRP3 signaling in primary GCs and relevant animal models, will be necessary to establish the causal roles of these pathways in GC senescence and ovarian aging. Furthermore, chromatin immunoprecipitation, promoter-binding assays and targeted WT1 perturbation will help determine whether WT1 directly regulates CDKN1A transcription during GC senescence. Moreover, integrating scATAC-seq (34) and spatial transcriptomics (35) could further elucidate the regulatory elements and spatial context of gene expression alterations during ovarian aging. Collectively, these approaches may help refine the mechanistic

framework of ovarian aging and facilitate the development of immune-modulatory and transcription-targeted strategies to preserve ovarian function.

In conclusion, the present study provides a high-resolution single-cell transcriptomic atlas of ovarian aging, revealing key cellular subpopulations and molecular pathways associated with reproductive decline. The identification of NLRP3+ macrophages and GC_Aged GCs, together with enhanced IL-1β-IL-1R1 signaling and WT1-associated transcriptional reprogramming, suggests that immune-endocrine interactions may contribute importantly to ovarian aging. These findings provide new insight into the cellular and molecular basis of ovarian aging and identify candidate targets for future therapeutic strategies aimed at preserving ovarian function and female fertility.

Acknowledgements

Not applicable.

Funding

The present study was supported by the following funding sources: The National Natural Science Foundation of China (grant no. 82501955); the Hebei Provincial Central Government-Guided Local Science and Technology Development Fund Project (Science and Technology Innovation Base Project) (grant no. 236Z7756G); the Natural Science Foundation of Hebei Province (grant no. H2024206427); the Natural Science Foundation of Hebei Province (grant no. H2023206356); the Natural Science Foundation of Hebei Province (grant no. H2024206433); the 2024 Hebei Provincial Government-Sponsored Clinical Medicine Outstanding Talent Training Program, (grant no. ZF2024040); and the 2025 Hebei Provincial Government-Sponsored Clinical Medicine Outstanding Talent Training Program (grant no. ZF2025102).

Availability of data and materials

The data generated in the present study may be requested from the corresponding author.

Authors' contributions

YD, CZ, ZL, JZ and XH conceived and designed the study. YD, CZ and YT conducted the experiments and wrote the manuscript. YD were responsible for data analysis and figure preparation. YD, ZL and XH discussed and revised the manuscript. XH and ZL reviewed and finalized the manuscript. All authors have read and approved the final manuscript. XH, and ZL are the corresponding authors and confirm the authenticity of all the raw data.

Ethics approval and consent to participate

The principles outlined in the Declaration of Helsinki and the Guidelines for the Care and Use of Laboratory Animals of the Chinese Institute of Health were strictly adhered to in the present study. The authors also complied with the ARRIVE guidelines. Ethical approval for the animal experiments was obtained from the Ethical Committee of Second Hospital of Hebei Medical University (approval no. 2021-AE034). All animal experiments conducted in the present study followed the guidelines and regulations specified in this ethical approval.

Patient consent for publication

Not applicable.

Competing interests

The authors declare that they have no competing interest.

References

1. Igarashi H, Takahashi T and Nagase S: Oocyte aging underlies female reproductive aging: Biological mechanisms and therapeutic strategies. Reprod Med Biol 14: 159-169, 2015.
2. Ahmed TA, Ahmed SM, El-Gammal Z, Shouman S, Ahmed A, Mansour R and El-Badri N: Oocyte aging: The role of cellular and environmental factors and impact on female fertility. Adv Exp Med Biol 1247: 109-123, 2020.
3. Richardson MC, Guo M, Fauser BCJM and Macklon NS: Environmental and developmental origins of ovarian reserve. Hum Reprod Update 20: 353-369, 2014.
4. Quinn MM and Cedars MI: Cardiovascular health and ovarian aging. Fertil Steril 110: 790-793, 2018.
5. Li L and Wang Z: Ovarian aging and osteoporosis. Adv Exp Med Biol 1086: 199-215, 2018.
6. Stachowiak G, Pertyński T and Pertyńska-Marczewska M: Metabolic disorders in menopause. Prz Menopauzalny 14: 59-64, 2015.
7. Isola JVV, Hense JD, Osório CAP, Biswas S, Alberola-Ila J, Ocañas SR, Schneider A and Stout MB: Reproductive ageing: Inflammation, immune cells, and cellular senescence in the aging ovary. Reproduction 168: e230499, 2024.
8. Zeng Y, Wang C, Yang C, Shan X, Meng XQ and Zhang M: Unveiling the role of chronic inflammation in ovarian aging: Insights into mechanisms and clinical implications. Hum Reprod 39: 1599-1607, 2024.
9. Liang J, Gai S, Na X, Hu J, Zhao Z, Zi D, Na Z, Gao W, Bi F and Li D: Ovarian aging at single-cell resolution: Current paradigms and perspectives. Ageing Res Rev 110: 102807, 2025.
10. Ma L, Lu H, Chen R, Wu M, Jin Y, Zhang J and Wang S: Identification of key genes and potential new biomarkers for ovarian aging: A study based on RNA-sequencing data. Front Genet 11: 590660, 2020.
11. Zhou Z, Yang X, Pan Y, Shang L, Chen S, Yang J, Jin L, Zhang F and Wu Y: Temporal transcriptomic landscape of postnatal mouse ovaries reveals dynamic gene signatures associated with ovarian aging. Hum Mol Genet 30: 1941-1954, 2021.
12. Shen L, Liu J, Luo A and Wang S: The stromal microenvironment and ovarian aging: Mechanisms and therapeutic opportunities. J Ovarian Res 16: 237, 2023.
13. Wang S, Sun ST, Zhang XY, Ding HR, Yuan Y, He JJ, Wang MS, Yang B and Li YB: The evolution of single-cell RNA sequencing technology and application: Progress and perspectives. Int J Mol Sci 24: 2943, 2023.
14. Gong X, Zhang Y, Ai J and Li K: Application of single-cell RNA sequencing in ovarian development. Biomolecules 13: 47, 2022.
15. Wu R, Van der Hoek KH, Ryan NK, Norman RJ and Robker RL: Macrophage contributions to ovarian function. Hum Reprod Update 10: 119-133, 2004.
16. Orisaka M, Mizutani T, Miyazaki Y, Shirafuji A, Tamamura C, Fujita M, Tsuyoshi H and Yoshida Y: Chronic low-grade inflammation and ovarian dysfunction in women with polycystic ovarian syndrome, endometriosis, and aging. Front Endocrinol (Lausanne) 14: 1324429, 2023.
17. Dompe C, Kulus M, Stefańska K, Kranc W, Chermuła B, Bryl R, Pieńkowski W, Nawrocki MJ, Petitte JN, Stelmach B, *et al*: Human granulosa cells-stemness properties, molecular cross-talk and follicular angiogenesis. Cells 10: 1396, 2021.
18. Zhang D, Yu Y, Duan T and Zhou Q: The role of macrophages in reproductive-related diseases. Heliyon 8: e11686, 2022.

19. Camaioni A, Ucci MA, Campagnolo L, De Felici M and Klinger FG; Italian Society of Embryology, Reproduction and Research (SIERR): The process of ovarian aging: It is not just about oocytes and granulosa cells. J Assist Reprod Genet 39: 783-792, 2022.
20. Toska E and Roberts SGE: Mechanisms of transcriptional regulation by WT1 (Wilms' tumour 1). Biochem J 461: 15-32, 2014.
21. Wilm B and Muñoz-Chapuli R: The Role of WT1 in embryonic development and normal organ homeostasis. Methods Mol Biol 1467: 23-39, 2016.
22. Jin C, Wang X, Yang J, Kim S, Hudgins AD, Gamliel A, Pei M, Contreras D, Devos M, Guo Q, *et al*: Molecular and genetic insights into human ovarian aging from single-nuclei multi-omics analyses. Nat Aging 5: 275-290, 2025.
23. Livak KJ and Schmittgen TD: Analysis of relative gene expression data using real-time quantitative PCR and the 2(-Delta Delta C(T)) method. Methods 25: 402-408, 2001.
24. Navarro-Pando JM, Alcocer-Gómez E, Castejón-Vega B, Navarro-Villarán E, Condés-Hervás M, Mundi-Roldan M, Muntané J, Pérez-Pulido AJ, Bullon P, Wang C, *et al*: Inhibition of the NLRP3 inflammasome prevents ovarian aging. Sci Adv 7: eabc7409, 2021.
25. Tatone C and Amicarelli F: The aging ovary-the poor granulosa cells. Fertil Steril 99: 12-17, 2013.
26. Yan F, Zhao Q, Li Y, Zheng Z, Kong X, Shu C, Liu Y and Shi Y: The role of oxidative stress in ovarian aging: A review. J Ovarian Res 15: 100, 2022.
27. Tanaka T, Urata Y, Harada M, Kunitomi C, Kusamoto A, Koike H, Xu Z, Sakaguchi N, Tsuchida C, Komura A, *et al*: Cellular senescence of granulosa cells in the pathogenesis of polycystic ovary syndrome. Mol Hum Reprod 30: gaae015, 2024.
28. Lu J, Zhang X, Liu H and Liu Y: Exploring the multifaceted role of WT1 in kidney development and disease. Kidney Blood Press Res 50: 176-188, 2025.
29. Tang W, Wang K, Feng Y, Tsui KH, Singh KK, Stout MB, Wang S and Wu M: Exploration of the mechanism and therapy of ovarian aging by targeting cellular senescence. Life Med 4: lnaf004, 2025.
30. Liang R, Qi X, Cai Q, Niu L, Huang X, Zhang D, Ling J, Wu Y, Chen Y, Yang P, *et al*: The role of NLRP3 inflammasome in aging and age-related diseases. Immun Ageing 21: 14, 2024.
31. Isola JVV, Ocañas SR, Hubbart CR, Ko S, Mondal SA, Hense JD, Carter HNC, Schneider A, Kovats S, Alberola-Ila J, *et al*: A single-cell atlas of the aging mouse ovary. Nat Aging 4: 145-162, 2024.
32. Zhou C, Guo Q, Lin J, Wang M, Zeng Z, Li Y, Li X, Xiang Y, Liang Q, Liu J, *et al*: Single-cell atlas of human ovaries reveals the role of the pyroptotic macrophage in ovarian aging. Adv Sci (Weinh) 11: e2305175, 2024.
33. Wang S, Zheng Y, Li J, Yu Y, Zhang W, Song M, Liu Z, Min Z, Hu H, Jing Y, *et al*: Single-cell transcriptomic atlas of primate ovarian aging. Cell 180: 585-600.e19, 2020.
34. Jansen C, Ramirez RN, El-Ali NC, Gomez-Cabrero D, Tegner J, Merkenschlager M, Conesa A and Mortazavi A: Building gene regulatory networks from scATAC-seq and scRNA-seq using linked self organizing maps. PLoS Comput Biol 15: e1006555, 2019.
35. Williams CG, Lee HJ, Asatsuma T, Vento-Tormo R and Haque A: An introduction to spatial transcriptomics for biomedical research. Genome Med 14: 68, 2022.